Principal Component Analysis of Data from NMR Titration Experiment of Uniformly ^{15}N Labelled Amyloid Beta (1–42) Peptide with Osmolytes and Phenolic Compounds

Naoko Iwaya[1,2,#], Natsuko Goda[2,#], Mizuki Matsuzaki[3], Akihiro Narita[3], Yoshiki Shigemitsu[2,4], Takeshi Tenno[2,3], Yoshito Abe[5], Minako Hoshi[6], and Hidekazu Hiroaki[2,3,*]

[1] Research Fellowship for Young Scientists, Japan Society for the Promotion of Science, Japan

[2] Laboratory of Structural Molecular Pharmacology, Graduate School of Pharmaceutical Sciences, Nagoya University, Furocho, Chikusa-ku, Nagoya 464-8601, Japan;

E-Mails: iwaya.naoko.2x@kyoto-u.ac.jp (N.I.); tenno.natsuko@f.mbox.nagoya-u.ac.jp (N.G.); tenno.takeshi@e.mbox.nagoya-u.ac.jp (T.T.)

[3] Structural Biology Research Center and Division of Biological Sciences, Graduate School of Science, Nagoya University, Furocho, Chikusa-ku, Nagoya 464-8601, Japan;

E-Mails: matsuzaki.mizuki@a.mbox.nagoya-u.ac.jp (M.M.);

narita.akihiro@f.mbox.nagoya-u.ac.jp (A.N.)

[4] School of Life Science and Technology, Tokyo Institute of Technology, Nagatsuda, 4259, Midori-ku, Yokohama, Kanagawa 226-8503, Japan;

E-Mail: shigemitsu.y.aa@m.titech.ac.jp (Y.S.)

[5] Graduate School of Pharmaceutical Sciences, Kyushu University, Fukuoka, Japan;

E-Mail: abe@phar.kyushu-u.ac.jp (Y.A.)

[6] Institute of Biomedical Research and Innovation, Kobe 650-0047, Japan;

E-Mail: minako.hoshi.9w@lmls-kobe.org (M.H.)

# These authors equally contributed to this work.

* Correspondence: hiroaki.hidekazu@f.mbox.nagoya-u.ac.jp; Tel.: +81-52-789-4535; Fax: +81-52-747-6471

Highlight:

- Principal component analysis (PCA) was introduced to analyze chemical shift perturbation (CSP) experiment data.
- NMR titration of uniformly ^{15}N-labeled amyloid β (1-42) peptide with fibrilization inhibitors were analyzed.
- Conventional CSP analysis failed to distinguish the relevant binding residues.

- PCA diagram suggested that osmolytes induced structural change of Aβ peptide.

Abstract:

A simple NMR method to analyze the data obtained by NMR titration experiment of amyloid formation inhibitors against uniformly ^{15}N-labeled amyloid-β 1-42 peptide (Aβ(1-42)) was described. By using solution nuclear magnetic resonance (NMR) measurement, the simplest method for monitoring the effects of Aβ fibrilization inhibitors is the NMR chemical shift perturbation (CSP) experiment using ^{15}N-labeled Aβ(1–42). However, the flexible and dynamic nature of Aβ(1–42) monomer may hamper the interpretation of CSP data. Here we introduced principal component analysis (PCA) for visualizing and analyzing NMR data of Aβ(1–42) in the presence of amyloid inhibitors including high concentration osmolytes. We measured ^{1}H-^{15}N 2D spectra of Aβ(1–42) at various temperatures as well as of Aβ(1–42) with several inhibitors, and subjected all the data to PCA (PCA-HSQC). The PCA diagram succeeded in differentiating the various amyloid inhibitors, including epigallocatechin gallate (EGCg), rosmarinic acid (RA) and curcumin (CUR) from high concentration osmolytes. We hypothesized that the CSPs reflected the conformational equilibrium of intrinsically

disordered Aβ(1–42) induced by weak inhibitor binding rather than the specific molecular interactions.

Keywords

principal component analysis; solution NMR; amyloid fibril formation; Alzheimer's disease; real time thioflavin-T assay; chemical shift perturbation mapping

1. Introduction

Alzheimer's disease (AD) is one of the most common dementias among the aged population [1]. The characteristic pathology of AD includes the progressive deposition of amyloid-β proteins (Aβ) outside the neuron cells [2] and accumulation of insoluble aggregates of tau protein inside the neuron cells [3] in the patients' brains. These Aβ peptides commonly include Aβ(1–40) and Aβ(1–42), and are known to form amyloid fibrils and soluble oligomers, both toxic and less toxic [1,2,4–8].More than 300 small synthetic and naturally-occurring molecules have been reported as Aβ fibrilization inhibitors [9]. However, among these inhibitors, since different types of modes of action may exist in parallel (amyloid nucleation inhibition, amyloid growth inhibition, amyloid solubilization or oligomer formation inhibition), rational design of amyloid inhibitor seems difficult [9]. In the literatures, we found that only a limited number of reports mentioned Aβ(1–42) in terms of both a time-dependent fluorescence Thioflavin-T (ThT) assay and an interaction study using solution nuclear magnetic resonance (NMR), for example, a designed synthetic molecule CLR01 [10] and a flavonoid myricetin [11].

In this study, the amyloid fibril formation inhibitors shown in Figure 1 were systematically examined using two methods: a thioflavin T (ThT) fluorescence assay and a ^{1}H-^{15}N two-dimensional NMR study. These natural amyloid inhibitors include

epigallocatechin gallate (EGCg) [10,12], rosmarinic acid (RA) [11,13,14], and curcumin (CUR) [11,15](Figure 1). The ThT fluorescence assay was used to assess the ability of each compound to inhibit amyloid fibril formation. On the other hand, the NMR experiments with Aβ(1–42) monomer and amyloid inhibitors may indicate how the inhibitor influences the monomer peptide (for example, via specific or non-specific interaction). Although the NMR titration experiment (formerly also known as chemical shift perturbation (CSP) mapping experiment) is an excellent indicator of protein-ligand interfaces, it may fail to map the interface when the entire protein may change conformation, such as intrinsically flexible Aβ(1–42) peptide [16].

Herein, we introduced the principal component analysis (PCA) of NMR-CSP data instead of mapping to the surface of Aβ(1–42) peptide structure. The signal changes are possibly attributed to a shift in the equilibrium among multiple local conformations of the intrinsically disorder Aβ(1–42) monomer, rather than a direct interaction between the peptide and the compound.

2. Materials and Method

Preparation of ^{15}N-labeled Aβ(1–42) peptide and NMR experiments

To produce human Aβ(1–42) peptide, we used a pET-based *Escherichia coli* expression plasmid that carried a hexa-histidine tag and an N-terminal yeast ubiquitin tag. To produce ^{15}N-labeled Aβ(1–42), cells were grown at 37°C in 1 L of M9 minimal media containing $^{15}NH_4Cl$ as the sole nitrogen source, followed by Aβ(1–42), according to our previous report [17]. Unlabeled Aβ(1–42) was also prepared in the same manner. The purified peptides were lyophilized, re-dissolved in hexafluoroisopropanol at the concentration no greater than 100 μM, lyophilized again, and then stored at −20°C until use [17].

NMR experiments were conducted using Bruker Avance III and Avance (600 MHz) NMR spectrometers (Bruker, Karlsruhe, Germany) equipped with cryogenic triple-resonance TCI and TXI probes, respectively. The lyophilized Aβ(1–42) powder was first dissolved in a few d_6-dimethyl sulfoxide (DMSO) and then immediately diluted with the solution conditions for NMR. For the temperature shift experiments, a 75-μM sample of Aβ(1–42) was dissolved in 300 μL of 0.5× PBS (pH 7.4) containing 1% d_6-DMSO and 10% D_2O in a Shigemi NMR tube (Shigemi, Co. Ltd). Following this, ^{1}H–^{15}N HSQC or ^{1}H–^{15}N SOFAST-HMQC spectra [18] were recorded at five temperatures: 283 K, 288 K, 298 K, 303 K, and 310 K. We observed severe signal broadening at 303 K and 310 K, thereby omitting these two datasets from the following PCA calculation. For the inhibitor CSP study, a 75-

μM sample of Aβ(1–42) was dissolved in 300 μL of 0.5× PBS (pH 7.4) containing 1% d_6-DMSO and 10% D_2O, and ^1H–^{15}N HSQC spectra were measured in the presence of the indicated final concentration of ligand. Assignments for the Aβ(1–42) signals were taken from the literature [10,19]. For adding osmolytes to Aβ(1–42), pre-weighted lyophilized powder of trehalose (TRH), sucrose (SUC), and glucose (GLC.) were used. For adding natural inhibitors (scyllo-inositol (sINO), RA, CUR, and EGCg, 10 mM stock solution in d_6-DMSO were used. NMR CSP experiments were conducted at 283 K. All spectra were processed using NMRPipe software [20] and analyzed using SPARKY software [21]. CSP, also known as a normalized chemical shift change in the ^1H-^{15}N HSQC (SOFAST-HMQC) spectra upon addition of osmolytes or amyloid inhibitors were calculated as $CSP = \{\Delta\delta H^2 + [\Delta\delta N/6]^2\}^{1/2}$, where ΔδH and ΔδN are chemical shift changes in amide proton and amide nitrogen, respectively. We performed the titration experiments of the natural inhibitors with 37.5, 75, 375, and 750 μM (0.5, 1, 5, and 10 molecular equivalents, respectively). Except sINO, some precipitation was observed at higher concentration. For further analysis, the chemical shift data with a minimal obvious precipitation, 750 μM sINO, 375 μM EGCg, 75 μM RA, and 37.5 μM CUR, were used.

PCA of the ^1H–^{15}N HSQC spectra was performed according to the method of Sakurai et al. [22]. First, the chemical shift data from each spectrum were represented as

a one-dimensional vector that contains δN and δH values in this order. Both δN and δH values were normalized using the average and the standard deviation of the δN and δH values, respectively. Following this, 10 vectors (three from the temperature shift experiments and seven from the inhibitor CSP experiments) were concatenated to build a two-dimensional matrix. Some row vectors lacking standardized chemical shift data due to missing NMR signals were omitted before PCA. The matrix size was 66 [33 (number of traceable residues) × 2 (δH and δN)] × 10 (measured temperature and compound points). A standard singular value decomposition analysis was performed by using the "princomp" function of the program octave 3.8.0 and a statistics package [23].

Real-time ThT fluorescence assay

Fluorescence enhancement upon ThT binding to amyloid was recorded with the Hitachi F-7000 Fluorescence Spectrophotometer (Hitachi, Co. Ltd). An excitation wavelength of 440 nm and an emission wavelength of 484 nm were used. ThT and protein concentrations were 5 μM and 25 μM, respectively, according to our previous report [17]

Electron microscopy

For negatively stained electron microscopy, 25 μM (0.1mg/mL) Aβ(1–42) was allowed to form amyloid fibrils in 0.5× phosphate-buffered saline (PBS, pH 7.4) at 37°C (310K). 0.5× PBS was prepared from 20 times dilution of PBS (×10) solution purchased from Nacalai Tesque (Kyoto, Japan, cat. No. 27575-31). Aliquots (5 μL) of the solution before amyloid fibril formation and 60 min after amyloid fibril formation were stained on a glow-discharged, carbon-supported copper grid (elastic carbon substrate on STEM100Cu grids, 100-mm grid pitch, Okenshoji Co., Ltd, Tokyo, Japan). Sample staining was performed with 5 μL of 2% uranyl acetate, and the samples were washed then three times (total, 10 μL) with the uranyl acetate solution. Images were collected using a JEM-1200 EX-II microscope (JEOL, Co, Tokyo, Japan) operated at an acceleration voltage of 70 kV and recorded using Electron-Microscopic Film FG (FUJIFILM, Co Ltd, Tokyo, Japan).

Results

Quality control of *E. coli* derived recombinant Aβ(1–42) in terms of amyloid fibril formation by using electron microscopy

All Aβ(1–42) used in this study was prepared using an *E. coli* expression system in our laboratory. Finder et al. reported that *E. coli*-derived recombinant Aβ(1–42)

and the synthetic Aβ(1–42) showed different fibrilization time course, and *E. coli*-derived recombinant Aβ(1–42) may contain much more seeds for amyloid fibril formation [24,25]. Thus, before starting the experiments, we confirmed the quality of our recombinant Aβ(1–42) sample. As shown in Figure 2A, we succeeded in reproducing the reported phenomenon. Even without adding external seeds, our Aβ(1–42) peptide began to form amyloid 30 min after initiating the reaction (Figure 3, filled circle). The growth curve for the amyloid fibril formation clearly shows a typical sigmoidal process that includes three distinct phases: a lag phase, fibril growth phase, and plateau phase. We further confirmed the shapes of the amyloid fibrils using negatively stained electron microscopy. Figure 2A and B shows electron micrographs of the samples taken before and 60 min after starting the amyloid fibril formation reaction. In Figure 2B, we can readily see linear fibrils with a uniform diameter.

Real-time ThT fluorescence assays with selected natural amyloid fibril formation inhibitors

Next, we assessed the amyloid fibril formation inhibition activity of the known natural amyloid inhibitors listed in Figure 1. In this study, we selected several compounds whose amyloid inhibition activity has already been reported in the

literature [11,26–29]. Nevertheless, we found that the real-time ThT fluorescent assay data were not completely accumulated for all amyloid inhibitors. We are aware of the importance of the profile of real-time ThT assay, because it is useful to discriminate whether the inhibitors affect nucleation phase or elongation phase of amyloid fibril formation [30]. However, experimental reproducibility of *in vitro* fibril formation is sensitive for many initial conditions, such as the molecular species examined [Aβ(1–40) or Aβ(1–42)], peptide concentration, temperature, buffer conditions, and amounts of pre-existing amyloid seeds in the sample [17]. Therefore, we performed real-time ThT assays for each of the amyloid inhibitors (Figure 1) under unified conditions (Figure 3A and 3B).

First, we focused on a series of sugars, including TRH, SUC, and GLC. The effects of sugars on proteins have been widely investigated. These sugars are known as osmolytes; they may stabilize the native state of the protein through preferential hydration mechanisms [31–38]. In our previous study, we reported that fibrillation of Aβ(1–42) was attenuated by 1.5 M SUC after incubation for 60 h under physiological conditions [28]. Other articles reported that 250 mM TRH and SUC could suppress membrane damage induced by an Aβ oligomer. Under the unified conditions used in this study, High concentrations of TRH and SUC generally suppressed amyloid fibril

formation, whereas GLC showed only partial inhibition (Figure 3A). Lower (100 mM and 250 mM) sugar concentrations were also examined (data not shown). Under these conditions, the inhibitory activity of SUC was weaker than that of TRH. Thus, the amyloid inhibition activity of these sugars can be placed in the following order: TRH > SUC > GLC. In case of addition of 0.5M GLC, amyloid formation was only partially inhibited.

Accordingly, we compared the activities of the selected natural amyloid inhibitors that inhibit fibril formation (Figure 1). Interestingly, sINO did not inhibit amyloid fibril formation under our experimental conditions. Instead, sINO seemingly accelerated amyloid fibril formation (Figure 3B). RA also failed to inhibit, however, RA at the indicated concentration showed a certain delay of the lag phase, suggesting partial inhibition of nucleation process as well as fibril elongation [39]. EGCg was the most potent inhibitor in this study. We intended to apply the same method to CUR but failed because the strong UV absorption of CUR overlaps the excitation wavelength for ThT fluorescence.

2.3. Variety of chemical shift changes of Aβ(1–42) upon temperature shift and inhibitor addition (CSP experiment)

^{1}H-^{15}N NMR spectra of Aβ(1–42) as well as Aβ(1–40) showed a narrow signal dispersion that is typical for IDPs [40]. Among the many NMR analyses of Aβ(1–40) in solution, Yamaguchi et al. reported a unique temperature-dependent behavior of Aβ(1–40) [41]. In detail, the HSQC signals of Aβ(1–40) underwent unusual temperature-dependent changes in both their chemical shifts and signal intensities. A severe signal broadening at higher temperature is attributed to a shift in the dynamic equilibrium between the random coil state and the local short β-turn state [41]. In this study, we succeeded in reproducing the phenomenon with our recombinant Aβ(1–42) (Figure 4A).

Next, we performed the NMR CSP experiment using ^{15}N-labeled Aβ(1–42) by titrating the natural amyloid inhibitors. From these NMR CSP experiments, it was demonstrated that the interactions between Aβ(1-42) and the selected amyloid inhibitors were in the fast exchange regime. It should be noted that (1) in most cases, the chemical shift changes induced by the compounds are smaller than that induced by the temperature change, (2) the chemical shift changes were widely distributed over the entire molecule of Aβ(1-42), and (3) the residues exhibited the temperature-induced changes and that of the compounds-induced changes are overlapped (Figure 5). In Figure 5, the selected normalized chemical shift changes upon temperature change, addition of osmolyte (TRH) and polyphenols (EGCg, RA and CUR) are plotted against

the residue number of Aβ(1-42). Although each chemicals have different chemical structures and their molecular sizes, chemical shift changes were observed along the whole Aβ(1-42) residues. Based on these data, we failed to identify the critical binding residues of Aβ(1-42) to CUR, RA, and EGCg. We assume that CSP may reflect both the structural change of intrinsically disordered Aβ(1-42) peptide upon addition of chemicals as well as the direct interaction to the inhibitors. We hypothesized that this difficulty may due to the nature of Aβ(1–42) as an IDP. If Aβ(1–42) would adopt a single stable globular conformation in solution, such the chemical shift changes upon compounds titration is readily explained as the result of the specific molecular interactions. As an IDP, Aβ(1–42) exists in a dynamic equilibrium among many semi-stable conformations, but does not adopt to a single conformation. Only the time-averaged chemical shifts of these states are being observed. Thus, we analyzed the NMR spectra of CSP experiments and temperature-shift experiments together using a PCA method, instead of a chemical-shift-mapping representation (PCA-HSQC method, Figure 6).

2.4. Performance and limitation of the PCA-HSQC method

The use of a PCA method for the analysis of a series of spectra is essentially identical to a singular value decomposition (SVD) analysis assuming that each spectrum is a linear combination of a few basis spectra. In NMR, this assumption is always valid when they are in the fast exchange regime with respect to NMR chemical shift timescale. This case is very likely that the exchange regime is fast and reversible, therefore the case of Aβ(1-42) and the compounds meets the criteria above. We are referring to the report by Sakurai et al., who successfully introduced the PCA method during their analysis of the protein folding intermediate of βMG [22,42], with slight modification. After performing a singular value decomposition, we succeeded in obtaining 10 components and their corresponding contribution ratios. The contribution ratios of the first three principal components were 99.23 %, 0.74 %, and 0.02 %, respectively, and the sum of these three principal components was 99.99 %. Notably, relatively large contribution ratio of PC1 (> 85 %) was also reported by Sakurai et al [22]. After PCA analysis, all 10 normalized HSQC spectra data have the same PC1 values (PC1 = 0.32). The PC1 may represent the average spectrum of all the spectra analyzed, and the characteristic values according to the CSP are expressed by PC2 and PC3. Accordingly, we represented each data point using these three principal components and visualized the data as a 2D scattered graph only using PC2 and PC3 (Figure 6).

3. Discussion

In this study, we focused that the order of amyloid inhibitory activity of the three osmolytes (TRH > SUC > GLU) are well consistent to the order of their potential of preferential hydration. These osmolytes are active only at very high (> 250 mM) concentration. Under high osmolyte condition, preferential hydration effectively contributes to protein stability of folded proteins. Our previous study demonstrated that amyloid fibril formation of AL amyloidosis retarded under high sugar concentration condition because compact native-like structure were stabilized by preferential hydration. In preferential hydration theory, both exclusion of osmolyte and delivery of water are occurred at protein surface of unfolded state rather than native state. This water compulsion may also be occurred around intrinsically unstructured Aβ(1-42) preferentially. Therefore, we assumed that the amyloid inhibitor activity of the osmolytes should be attributed to their stabilizing action to the "native-like" structure. Even if Aβ(1-42) is an IDP that does not adopt into any of fixed conformations, the osmolytes can stabilize some of the possible "transient" compact conformations by water compulsion, resulting in amyloid fibril formation inhibition.

Figure 6 demonstrated that the data points including the temperature shift experiments and the osmolyte CSP experiments are categorized into two major series along the two lines. The first line includes temperature shift experiments, and the second line contains compound-induced CSP experiments with osmolytes. The first data series are roughly parallel to PC2 axis, whereas the second data series lie along the PC3 axis. In other words, although many residues of Aβ(1-42) exhibited both the compound-induced and the temperature-induced chemical shift changes, these two distinct physicochemical events were well separated by PCA. In addition, the similar tendency of the osmolytes-induced chemical shift changes observed in this study is readily visualized in the PCA diagram. The effects of the osmolytes upon Aβ(1-42) are thus discriminated from the other perturbations, such as the temperature shifts and EGCg. In contrast, all the other polyphenolic compounds in this study (except for sINO), are plotted at different positions from the former two data series, the temperature shift experiments and the osmolytes CSP experiments. Notably, the two phenolic compounds RA and CUR are both close to the red line, but opposite sides from the origin (the point of 0 eq, 10°C). This means that the residues indicated CSPs upon RA and CUR titration were mostly overlapped, whereas the signs of the induced chemical shift changes were

totally opposite, thereby suggesting the different molecular mechanism of amyloid inhibition.

Finally, this study showed a potential of the PCA-HSQC method to analyze the complicated effects of the various inhibitor on Aβ(1–42) HSQC signals during titrations. When focusing on the signal changes experienced by each residue in Aβ(1–42), a wide variety of spectral changes hampers our understanding of the overview of dynamic changes caused by each compound. According to this assumption, we hypothesized that the similarity and difference of HSQC spectra is useful to further discriminate the other amyloid inhibitors by their individual mechanism-on-action. For example, although some researchers pointed out the similarity of the chemical structure among RA, CUR, and EGCg, the mechanism of amyloid inhibition may be different, considering our results in PCA-HSQC method. In contrast, the real-time ThT assay profiles seems less informative to discriminate the mechanism-on-action of the amyloid inhibitors.

Acknowledgments

K. Tomii (AIST) for help with the PCA method. The authors thank Dr. S. Matsumoto (Kyoto University) and Dr. Y. O. Kamatari (Gifu University) for help with the NMR measurements. This study was supported by Grants-in-Aid from the Ministry of Education, Culture, Sports, Sciences and Technology (Grant No. 21113007), Grants-in-Aid from the Japan Society for the Promotion of Science (Grant No. 16K14707, 17H04055) and Grants-in-Aid for Nano Medicine (Grant No. H21-nano-007) from the Ministry of Health, Labor and Welfare. This work was supported by Salt Science Research Foundation (Grant No. 1222) and the Mishima-Kaiun Memorial Foundation (Grant No. H25-153) in Japan.

Conflict of Interest

The authors declare no competing financial interest.

Sample Availability: The expression vector of Aβ(1–42) is available from the authors.

References

[1] M. Prince, R. Bryce, E. Albanese, A. Wimo, W. Ribeiro, C.P. Ferri, The global prevalence of dementia: a systematic review and metaanalysis., Alzheimers. Dement. 9 (2013) 63-75.e2. https://doi.org/10.1016/j.jalz.2012.11.007.

[2] J. Hardy, D.J. Selkoe, The amyloid hypothesis of Alzheimer's disease: progress and problems on the road to therapeutics., Science. 297 (2002) 353–6.

https://doi.org/10.1126/science.1072994.

[3] A. Alonso, T. Zaidi, M. Novak, I. Grundke-Iqbal, K. Iqbal, Hyperphosphorylation induces self-assembly of tau into tangles of paired helical filaments/straight filaments., Proc. Natl. Acad. Sci. U. S. A. 98 (2001) 6923–8. https://doi.org/10.1073/pnas.121119298.

[4] M. Hoshi, M. Sato, S. Matsumoto, A. Noguchi, K. Yasutake, N. Yoshida, K. Sato, Spherical aggregates of beta-amyloid (amylospheroid) show high neurotoxicity and activate tau protein kinase I/glycogen synthase kinase-3beta., Proc. Natl. Acad. Sci. U. S. A. 100 (2003) 6370–6375. https://doi.org/10.1073/pnas.1237107100.

[5] R. Roychaudhuri, M. Yang, M.M. Hoshi, D.B. Teplow, Amyloid beta-protein assembly and Alzheimer disease., J. Biol. Chem. 284 (2009) 4749–53. https://doi.org/10.1074/jbc.R800036200.

[6] M. Sakono, T. Zako, Amyloid oligomers: formation and toxicity of Abeta oligomers., FEBS J. 277 (2010) 1348–1358. https://doi.org/10.1111/j.1742-4658.2010.07568.x.

[7] I. Benilova, E. Karran, B. De Strooper, The toxic Aβ oligomer and Alzheimer's disease: an emperor in need of clothes, Nat. Neurosci. 15 (2012) 349–357. https://doi.org/10.1038/nn.3028.

[8] T. Ohnishi, M. Yanazawa, T. Sasahara, Y. Kitamura, H. Hiroaki, Y. Fukazawa, I. Kii, T. Nishiyama, A. Kakita, H. Takeda, A. Takeuchi, Y. Arai, A. Ito, H. Komura, H. Hirao, K. Satomura, M. Inoue, S.-I.S. Muramatsu, K.K. Matsui, M. Tada, M. Sato, E. Saijo, Y. Shigemitsu, S. Sakai, Y. Umetsu, N. Goda, N. Takino, H. Takahashi, M. Hagiwara, T. Sawasaki, G. Iwasaki, Y. Nakamura, Y. Nabeshima, D.B.D.B. Teplow, M. Hoshi, T.C. Südhof, Na, K-ATPase α3 is a death target of Alzheimer patient amyloid-β assembly, Proc. Natl. Acad. Sci. 112 (2015) E4465–E4474. https://doi.org/10.1073/pnas.1421182112.

[9] B. Torok, S. Bag, M. Sarkar, S. Dasgupta, M. Torok, Structural features of small molecule amyloid-beta self-assembly inhibitors, Curr. Bioact. Compd. 9 (2013) 37–63. https://doi.org/10.2174/1573407211309010006.

[10] S. Sinha, Z. Du, P. Maiti, F.-G. Klärner, T. Schrader, C. Wang, G. Bitan, Comparison of three amyloid assembly inhibitors: the sugar scyllo-inositol, the polyphenol epigallocatechin gallate, and the molecular tweezer CLR01., ACS Chem. Neurosci. 3 (2012) 451–8. https://doi.org/10.1021/cn200133x.

[11] K. Ono, L. Li, Y. Takamura, Y. Yoshiike, L. Zhu, F. Han, X. Mao, T. Ikeda, J. Takasaki, H. Nishijo, A. Takashima, D.B. Teplow, M.G. Zagorski, M. Yamada, Phenolic compounds prevent amyloid β-protein oligomerization and synaptic dysfunction by site-specific binding., J. Biol. Chem. 287 (2012) 14631–43.

https://doi.org/10.1074/jbc.M111.325456.
[12] D.E. Ehrnhoefer, J. Bieschke, A. Boeddrich, M. Herbst, L. Masino, R. Lurz, S. Engemann, A. Pastore, E.E. Wanker, EGCG redirects amyloidogenic polypeptides into unstructured, off-pathway oligomers, Nat. Struct. Mol. Biol. 15 (2008) 558–566. https://doi.org/10.1038/nsmb.1437.
[13] C. Airoldi, C. Zona, E. Sironi, L. Colombo, M. Messa, D. Aurilia, M. Gregori, M. Masserini, M. Salmona, F. Nicotra, B. La Ferla, Curcumin derivatives as new ligands of Aβ peptides., J. Biotechnol. 156 (2010) 317–324. https://doi.org/10.1016/j.jbiotec.2011.07.021.
[14] C. Airoldi, E. Sironi, C. Dias, F. Marcelo, A. Martins, A.P. Rauter, F. Nicotra, J. Jimenez-Barbero, Natural compounds against Alzheimer's disease: molecular recognition of Aβ1-42 peptide by Salvia sclareoides extract and its major component, rosmarinic acid, as investigated by NMR., Chem. Asian J. 8 (2013) 596–602. https://doi.org/10.1002/asia.201201063.
[15] F. Yang, G.P. Lim, A.N. Begum, O.J. Ubeda, M.R. Simmons, S.S. Ambegaokar, P. Chen, R. Kayed, C.G. Glabe, S.A. Frautschy, G.M. Cole, Curcumin inhibits formation of amyloid β oligomers and fibrils, binds plaques, and reduces amyloid in vivo, J. Biol. Chem. 280 (2005) 5892–5901. https://doi.org/10.1074/jbc.M404751200.
[16] E.R.P. Zuiderweg, Mapping Protein−Protein Interactions in Solution by NMR Spectroscopy †, Biochemistry. 41 (2002) 1–7. https://doi.org/10.1021/bi011870b.
[17] Y. Shigemitsu, N. Iwaya, N. Goda, M. Matsuzaki, T. Tenno, A. Narita, M. Hoshi, H. Hiroaki, Nuclear magnetic resonance evidence for the dimer formation of beta amyloid peptide 1-42 in 1,1,1,3,3,3-hexafluoro-2-propanol., Anal. Biochem. 498 (2016) 59–67. https://doi.org/10.1016/j.ab.2015.12.021.
[18] P. Schanda, E. Kupce, B. Brutscher, Ē. Kupče, B. Brutscher, SOFAST-HMQC experiments for recording two-dimensional heteronuclear correlation spectra of proteins within a few seconds., J. Biomol. NMR. 33 (2005) 199–211. https://doi.org/10.1007/s10858-005-4425-x.
[19] Y. Yan, C. Wang, Abeta42 is more rigid than Abeta40 at the C terminus: implications for Abeta aggregation and toxicity., J. Mol. Biol. 364 (2006) 853–62. https://doi.org/10.1016/j.jmb.2006.09.046.
[20] F. Delaglio, S. Grzesiek, G.W. Vuister, G. Zhu, J. Pfeifer, A. Bax, NMRPipe: a multidimensional spectral processing system based on UNIX pipes., J. Biomol. NMR. 6 (1995) 277–293. http://www.ncbi.nlm.nih.gov/pubmed/8520220 (accessed March 9, 2012).
[21] T.D. Goddard, D.G. Kneller, Sparky 3, 2004, University of California, San

Francisco., (2004). http://www.cgl.ucsf.edu/home/sparky/.
[22] K. Sakurai, Y. Goto, Principal component analysis of the pH-dependent conformational transitions of bovine beta-lactoglobulin monitored by heteronuclear NMR., Proc. Natl. Acad. Sci. U. S. A. 104 (2007) 15346–51. https://doi.org/10.1073/pnas.0702112104.
[23] J.W. Eaton, GNU Octave, (1996). http://www.gnu.org/software/octave.
[24] M. Dasari, A. Espargaro, R. Sabate, J.M. Lopez del Amo, U. Fink, G. Grelle, J. Bieschke, S. Ventura, B. Reif, Bacterial inclusion bodies of Alzheimer's disease β-amyloid peptides can be employed to study native-like aggregation intermediate states., Chembiochem. 12 (2011) 407–23. https://doi.org/10.1002/cbic.201000602.
[25] V.H. Finder, I. Vodopivec, R.M. Nitsch, R. Glockshuber, The recombinant amyloid-beta peptide Abeta1-42 aggregates faster and is more neurotoxic than synthetic Abeta1-42., J. Mol. Biol. 396 (2010) 9–18. https://doi.org/10.1016/j.jmb.2009.12.016.
[26] W. Qi, A. Zhang, T.A. Good, E.J. Fernandez, Two Disaccharides and Trimethylamine N -Oxide Affect Aβ Aggregation Differently, but All Attenuate Oligomer-Induced Membrane Permeability, Biochemistry. 48 (2009) 8908–8919. https://doi.org/10.1021/bi9006397.
[27] J. McLaurin, R. Golomb, a Jurewicz, J.P. Antel, P.E. Fraser, Inositol stereoisomers stabilize an oligomeric aggregate of Alzheimer amyloid beta peptide and inhibit abeta -induced toxicity., J. Biol. Chem. 275 (2000) 18495–502. https://doi.org/10.1074/jbc.M906994199.
[28] T. Ueda, M. Nagata, A. Monji, I. Yoshida, N. Tashiro, T. Imoto, Effect of sucrose on formation of the beta-amyloid fibrils and D-aspartic acids in Abeta 1-42., Biol. Pharm. Bull. 25 (2002) 375–378. https://doi.org/10.1248/bpb.25.375.
[29] A. a Reinke, J.E. Gestwicki, Structure-activity relationships of amyloid beta-aggregation inhibitors based on curcumin: influence of linker length and flexibility., Chem. Biol. Drug Des. 70 (2007) 206–215. https://doi.org/10.1111/j.1747-0285.2007.00557.x.
[30] Y. Shigemitsu, H. Hiroaki, Common molecular pathogenesis of disease-related intrinsically disordered proteins revealed by NMR analysis, J. Biochem. 163 (2018) 11–18. https://doi.org/10.1093/jb/mvx056.
[31] M. Auton, D.W. Bolen, J. R??sgen, Structural thermodynamics of protein preferential solvation: Osmolyte solvation of proteins, aminoacids, and peptides, Proteins Struct. Funct. Genet. 73 (2008) 802–813. https://doi.org/10.1002/prot.22103.
[32] J.C. Lee, S.N. Timasheff, The stabilization of proteins by sucrose., J. Biol. Chem. 256 (1981) 7193–201. http://www.ncbi.nlm.nih.gov/pubmed/7251592 (accessed July

18, 2014).
[33] T. Arakawa, S.N. Timasheff, Stabilization of protein structure by sugars., Biochemistry. 21 (1982) 6536–6544. https://doi.org/10.1021/bi00268a033.
[34] T. Ueda, M. Nagata, T. Imoto, Aggregation and chemical reaction in hen lysozyme caused by heating at pH 6 are depressed by osmolytes, sucrose and trehalose., J. Biochem. 130 (2001) 491–496. https://doi.org/10.1093/oxfordjournals.jbchem.a003011.
[35] H. Hamada, T. Arakawa, K. Shiraki, Effect of additives on protein aggregation., Curr. Pharm. Biotechnol. 10 (2009) 400–7. http://wolfson.huji.ac.il/purification/PDF/Literature/Hamada2009.pdf (accessed June 1, 2012).
[36] O. Miyawaki, Hydration state change of proteins upon unfolding in sugar solutions, Biochim. Biophys. Acta - Proteins Proteomics. 1774 (2007) 928–935. https://doi.org/10.1016/j.bbapap.2007.05.008.
[37] M. Abe, Y. Abe, T. Ohkuri, T. Mishima, A. Monji, S. Kanba, T. Ueda, Mechanism for retardation of amyloid fibril formation by sugars in Vλ6 protein., Protein Sci. 22 (2013) 467–74. https://doi.org/10.1002/pro.2228.
[38] Y. Abe, N. Odawara, N. Aeimhirunkailas, H. Shibata, N. Fujisaki, H. Tachibana, T. Ueda, Inhibition of amyloid fibril formation in the variable domain of λ6 light chain mutant Wil caused by the interaction between its unfolded state and epigallocatechin-3-O-gallate, Biochim. Biophys. Acta - Gen. Subj. (2018). https://doi.org/10.1016/j.bbagen.2018.08.006.
[39] M.R. Wilson, J.J. Yerbury, S. Poon, Potential roles of abundant extracellular chaperones in the control of amyloid formation and toxicity., Mol. Biosyst. 4 (2008) 42–52. https://doi.org/10.1039/b712728f.
[40] H. Hiroaki, Y. Umetsu, Y. Nabeshima, M. Hoshi, D. Kohda, A simplified recipe for assigning amide NMR signals using combinatorial 14N amino acid inverse-labeling., J. Struct. Funct. Genomics. 12 (2011) 167–174. https://doi.org/10.1007/s10969-011-9116-0.
[41] T. Yamaguchi, K. Matsuzaki, M. Hoshino, Transient formation of intermediate conformational states of amyloid-β peptide revealed by heteronuclear magnetic resonance spectroscopy., FEBS Lett. 585 (2011) 1097–102. https://doi.org/10.1016/j.febslet.2011.03.014.
[42] K. Sakurai, A. Maeno, Y.H. Lee, K. Akasaka, Conformational Properties Relevant to the Amyloidogenicity of β 2 -Microglobulin Analyzed Using Pressure- and Salt-Dependent Chemical Shift Data, J. Phys. Chem. B. 123 (2019) 836–844. https://doi.org/10.1021/acs.jpcb.8b11408.

Figure legends

Figure 1. Structures of β-amyloid fibril formation inhibitors used in this study.

Figure 2. Negatively stained electron microscopic analysis of the bacterially expressed Aβ(1–42) used in this study. Samples were analyzed before amyloid fibril formation (A) and 60 min after the initiation of amyloid fibril formation (B). Scale bars represent 500 nm.

Figure 3. Real-time ThT fluorescence assay for the inhibition of β-amyloid fibril formation. The inhibitors and concentrations used are shown in the figure. (A) Effect of osmolytes GLC (0.5 M, gray diamond), SUC (0.5 M, closed triangle), TRH (0.5 M, gray square), and Aβ(1–42) alone (closed circle). (B) Effect of amyloid fibril formation inhibitors sINO (100 μM, gray square), RA (25 μM, cross), EGCg (100 μM, closed triangle), and Aβ(1–42) alone (closed circle).

Figure 4. Expanded HSQC spectra of ^{15}N-labeled Aβ(1–42). (**A**) Overlay of HSQC spectra measured at various temperatures. Spectra recorded at 283 K (black), 288 K (blue), 298 K (orange), 303 K (green), and 310 K (purple) were overlaid. (**B**) Overlay of HSQC spectra with 500 mM osmolytes measured at 283K. Aβ(1–42) with GLC (purple), SUC (orange), TRH (cyan), and Aβ(1–42) alone (black). (**C**) Overlay of HSQC spectra

with 750 μM (1:10) sINO (magenta), 75 μM (1:1) RA (green), 37.5 μM (1:0.5) CUR (blue), 375 μM (1:5) EGCg (orange), and Aβ(1–42) alone (black).

Figure 5. Normalized chemical shift changes of the ^{1}H-^{15}N NMR spectra of 15N-labeled Aβ(1–42) upon temperature shift or addition of chemicals. black, temperature shift (from 283K to 285K); red, 0.5 M TRH; light green, 375 μM (1:5) EGCg; magenta, 75 μM (1:1) RA; sky blue; 37.5 μM (1:0.5) CUR.

Figure 6. A 2D scatter plot of the ^{1}H-^{15}N NMR spectra of ^{15}N-labeled Aβ(1–42) analyzed by principal component analysis. The sample conditions (i.e., temperature in temperature shift experiments and compound with a given concentration for inhibitor CSP experiments) are labeled in the figure. The plots for 10°, 0 eq of compounds and for 750 μM sINO were overlapped.

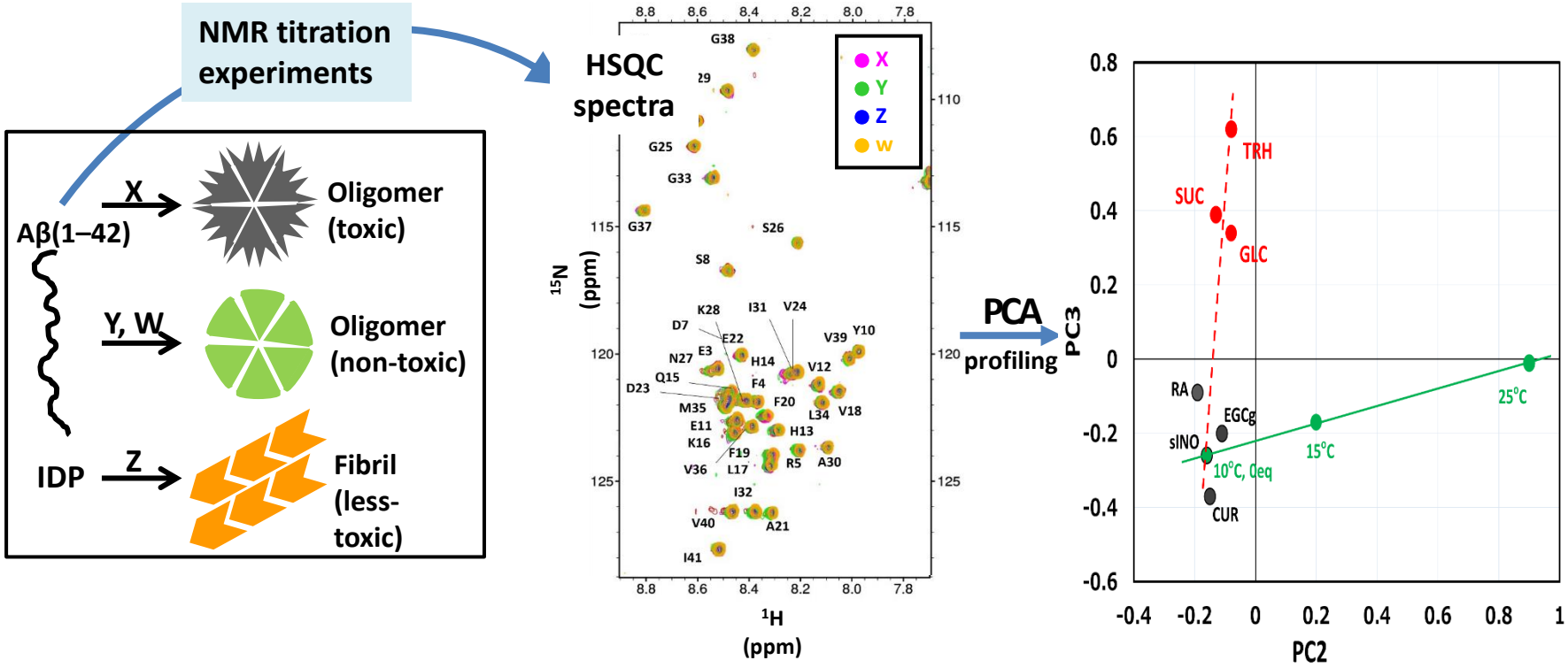
NMR titration experiments
Aβ(1–42)
X
Oligomer (toxic)
Y, W
Oligomer (non-toxic)
IDP
Z
Fibril (less-toxic)
HSQC spectra
X
Y
Z
W
^{15}N (ppm)
^{1}H (ppm)
PCA profiling
PC3
PC2
TRH
SUC
GLC
RA
EGCg
slNO
CUR
10°C, 0eq
15°C
25°C

TOC-revised

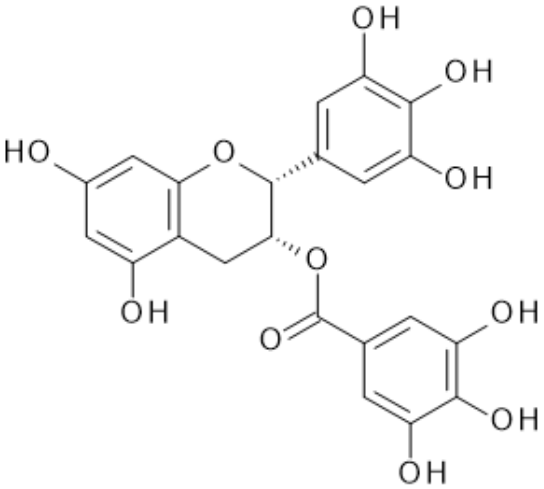

EGCg : (-)-Epigallocatechin gallate

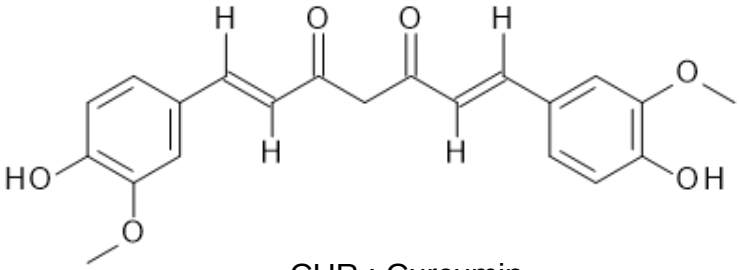

CUR : Curcumin

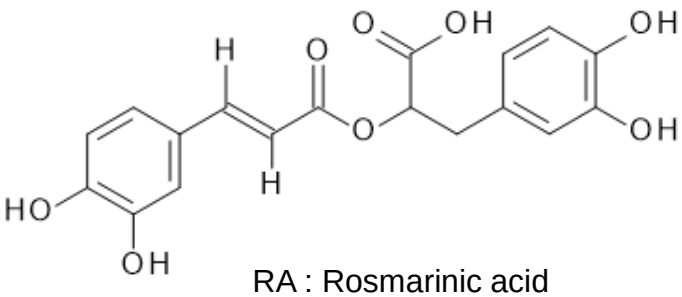

RA : Rosmarinic acid

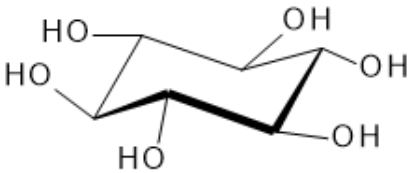

sINO : scyllo-Inositol

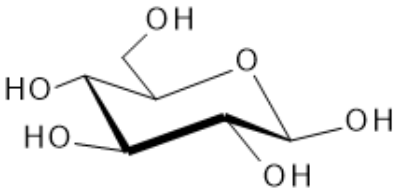

GLC : Glucose

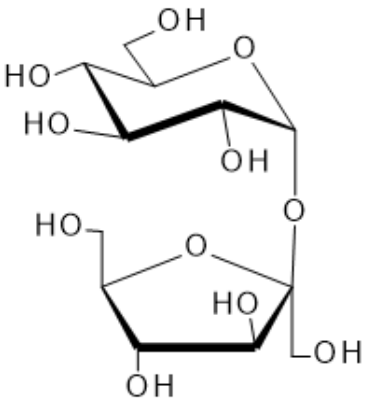

SUC : Sucrose

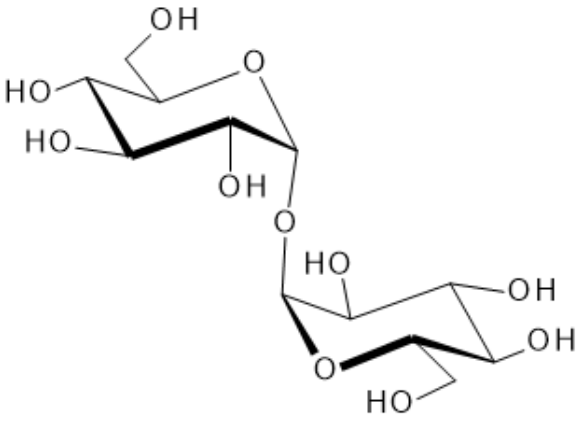

TRH : Trehalose

Figure 1

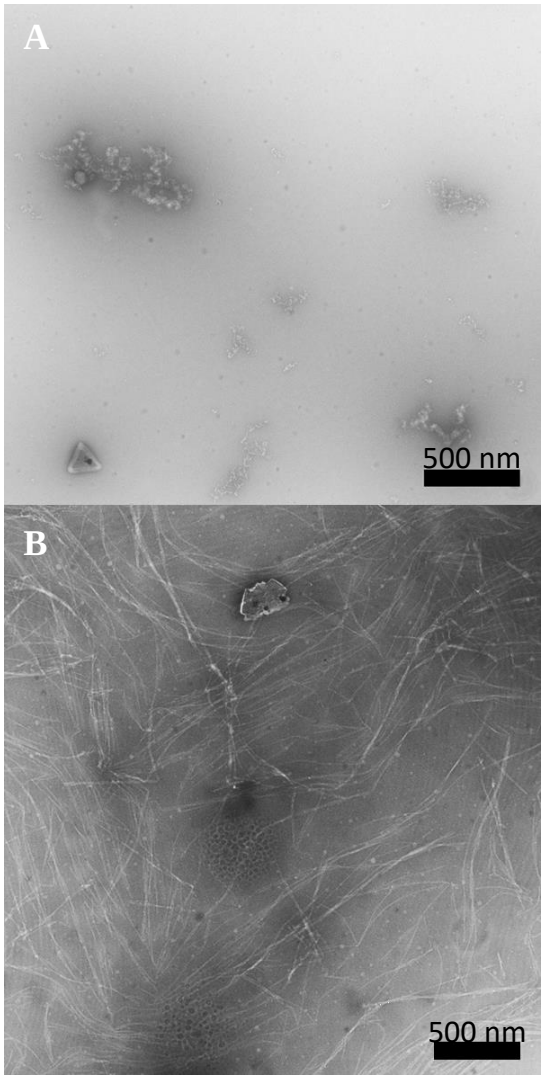

Figure 2

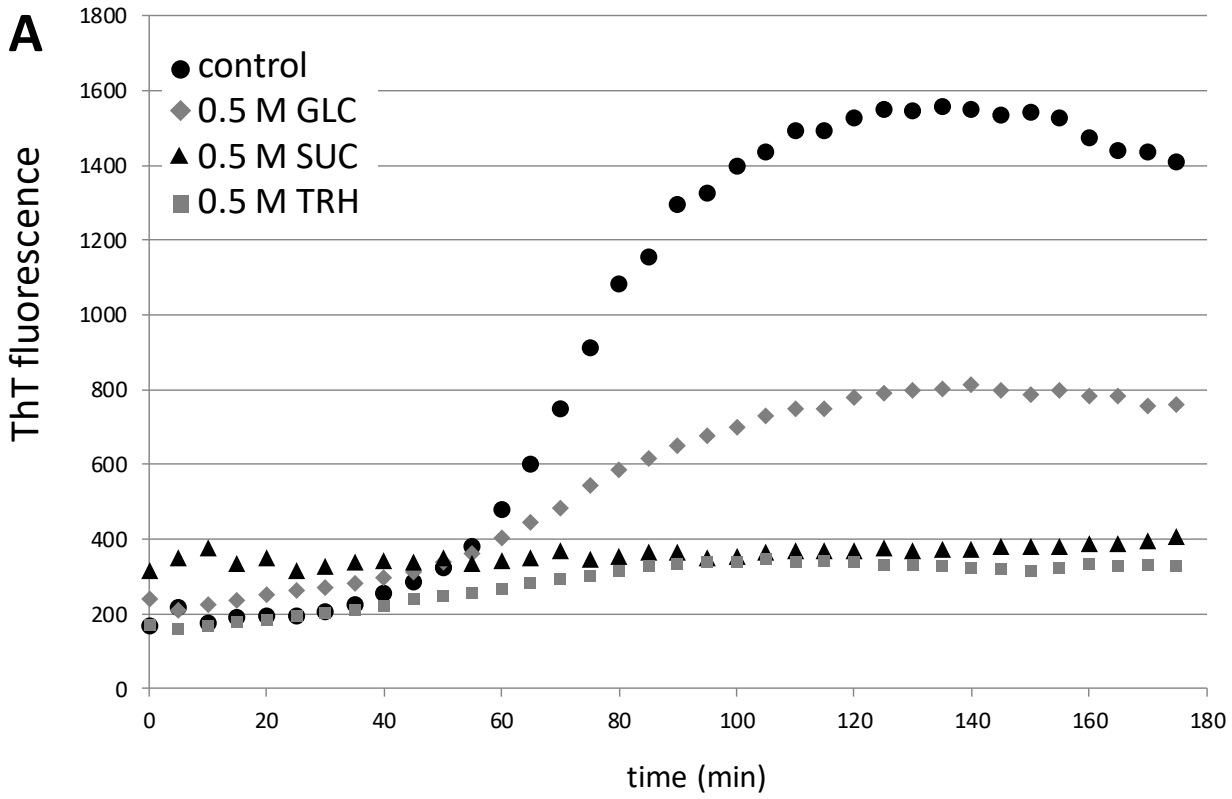
A
control
0.5 M GLC
0.5 M SUC
0.5 M TRH
ThT fluorescence
time (min)
0
200
400
600
800
1000
1200
1400
1600
1800
0
20
40
60
80
100
120
140
160
180

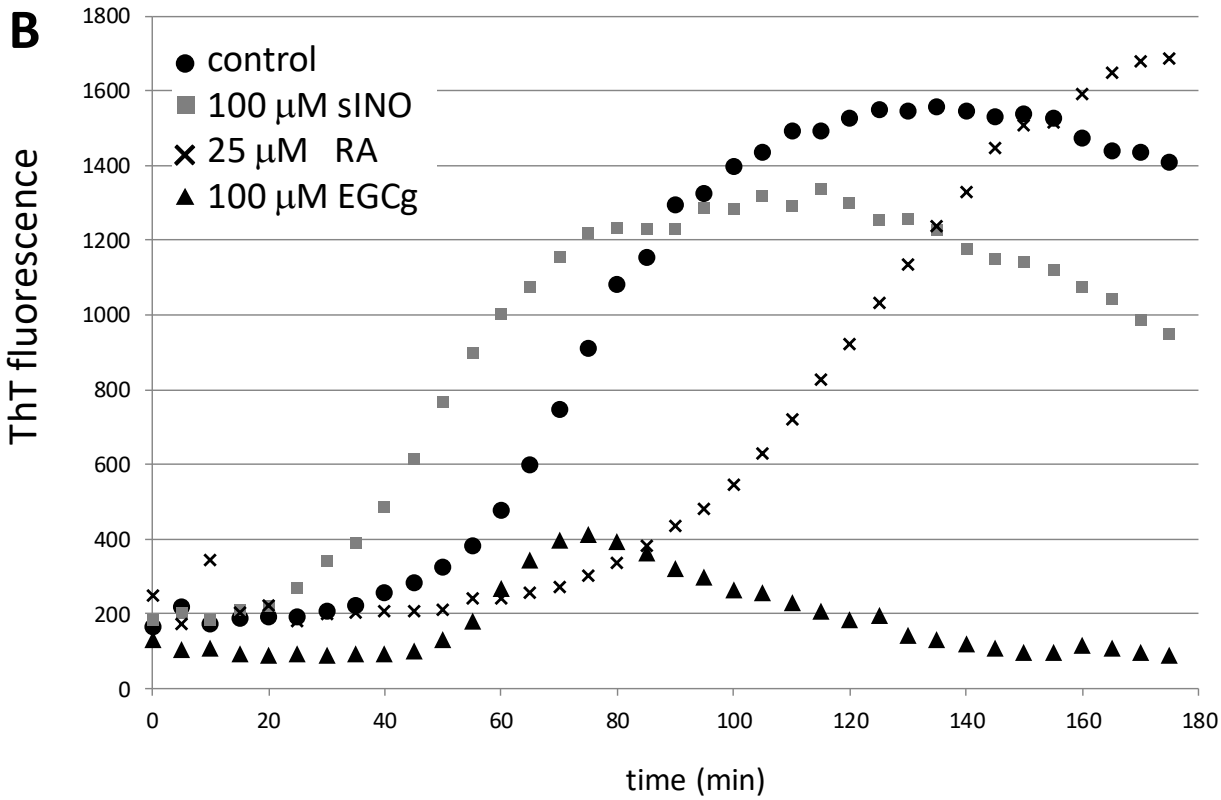
B
control
100 µM sINO
25 µM RA
100 µM EGCg
ThT fluorescence
time (min)
0
200
400
600
800
1000
1200
1400
1600
1800
0
20
40
60
80
100
120
140
160
180

Figure 3

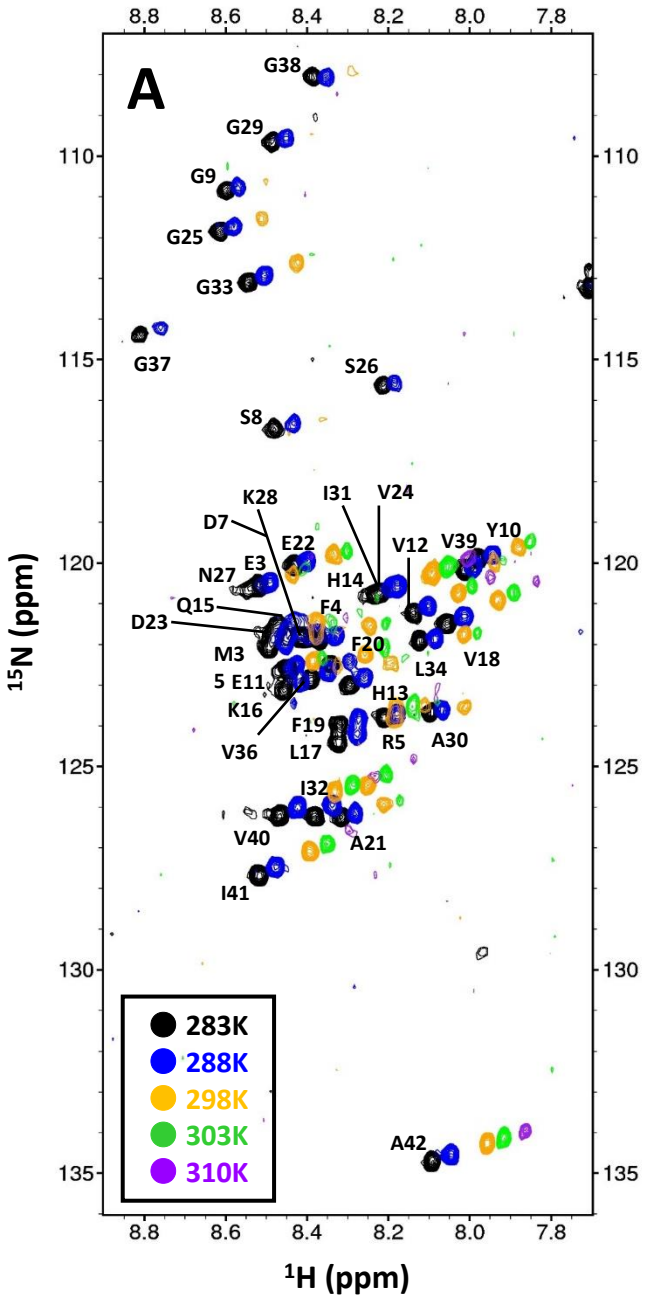
A
8.8
8.6
8.4
8.2
8.0
7.8
110
115
120
125
130
135
^{15}N (ppm)
^{1}H (ppm)
G38
G29
G9
G25
G33
G37
S26
S8
K28
I31
V24
D7
E22
V12
V39
Y10
E3
N27
H14
Q15
F4
D23
F20
M3
L34
V18
5 E11
H13
K16
F19
R5
A30
V36
L17
I32
V40
A21
I41
A42
283K
288K
298K
303K
310K

Figure 4(A)

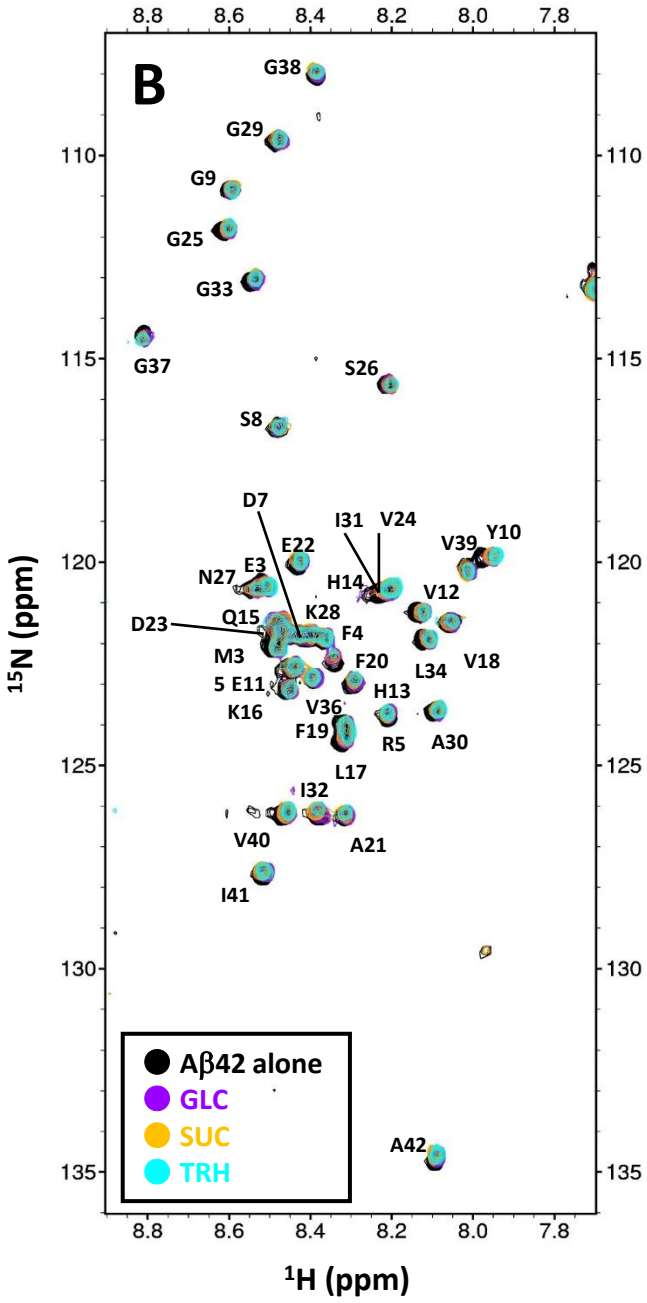
B
G38
G29
G9
G25
G33
G37
S26
S8
D7
I31
V24
E22
V39
Y10
E3
N27
H14
V12
Q15
K28
D23
F4
M3
F20
L34
V18
5 E11
H13
K16
V36
F19
R5
A30
L17
I32
V40
A21
I41
A42
Aβ42 alone
GLC
SUC
TRH
8.8
8.6
8.4
8.2
8.0
7.8
110
115
120
125
130
135
15N (ppm)
1H (ppm)

Figure 4(B)

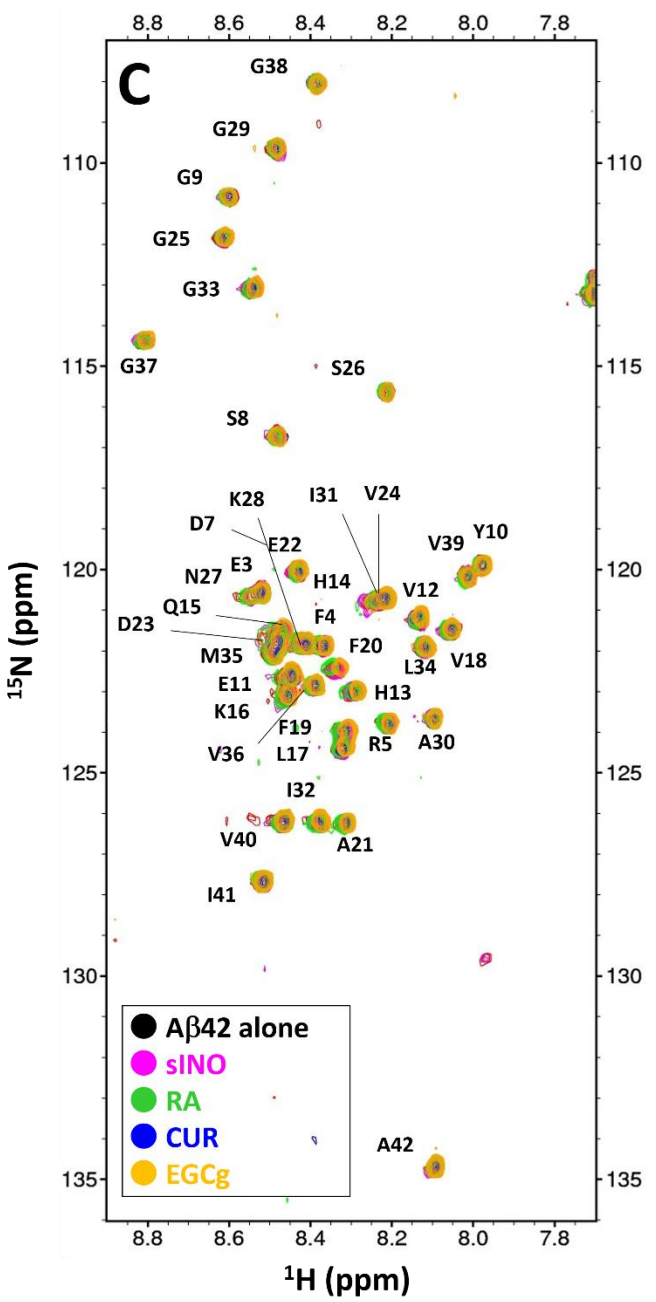
C
G38
G29
G9
G25
G33
G37
S26
S8
K28
I31
V24
D7
E22
V39
Y10
E3
N27
H14
V12
Q15
F4
D23
F20
L34
V18
M35
E11
H13
K16
F19
R5
A30
V36
L17
I32
V40
A21
I41
A42
Aβ42 alone
sINO
RA
CUR
EGCg
8.8
8.6
8.4
8.2
8.0
7.8
110
115
120
125
130
135
^{15}N (ppm)
^{1}H (ppm)

Figure 4(C)

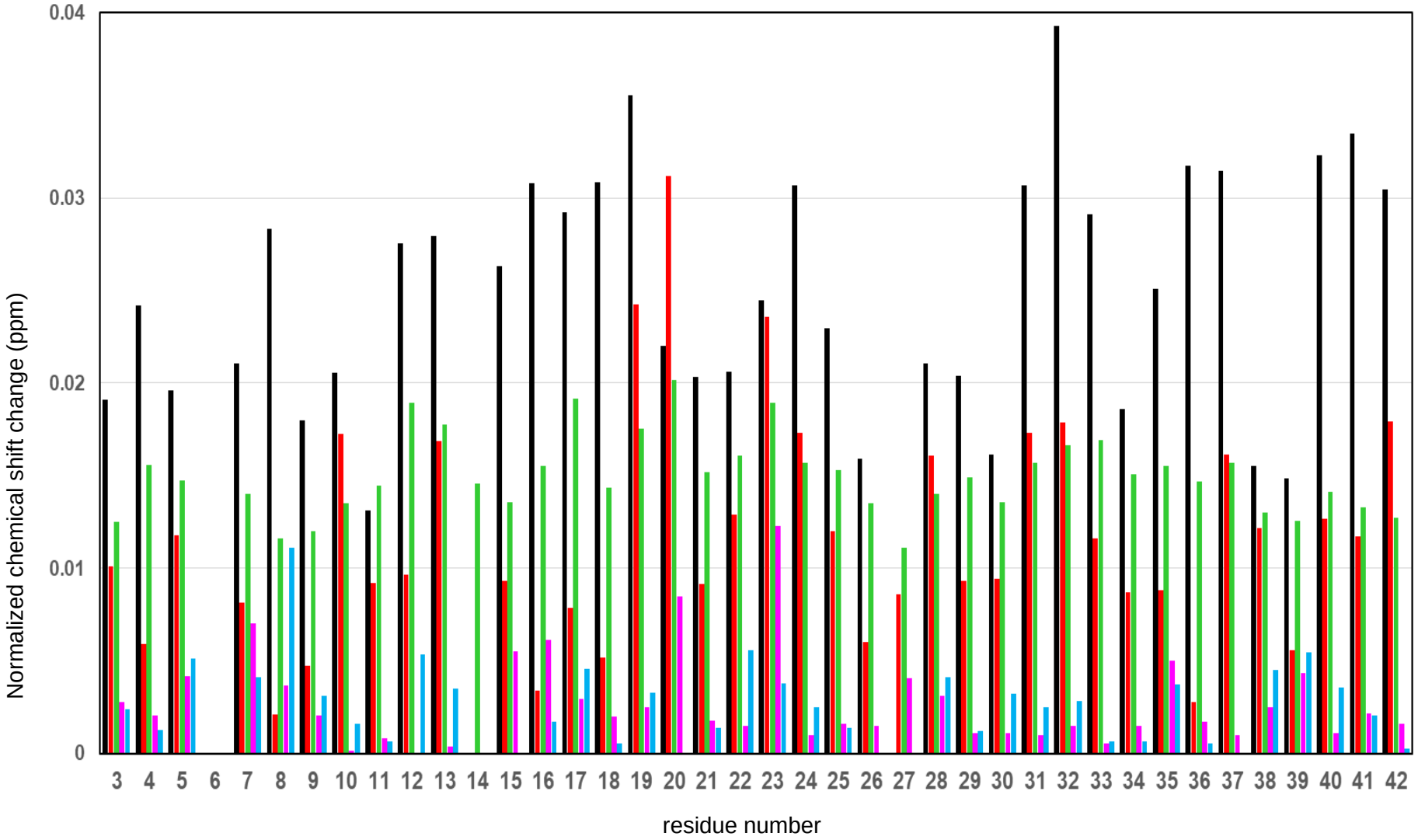
0.04
0.03
0.02
0.01
0
Normalized chemical shift change (ppm)
3 4 5 6 7 8 9 10 11 12 13 14 15 16 17 18 19 20 21 22 23 24 25 26 27 28 29 30 31 32 33 34 35 36 37 38 39 40 41 42
residue number

Figure 5

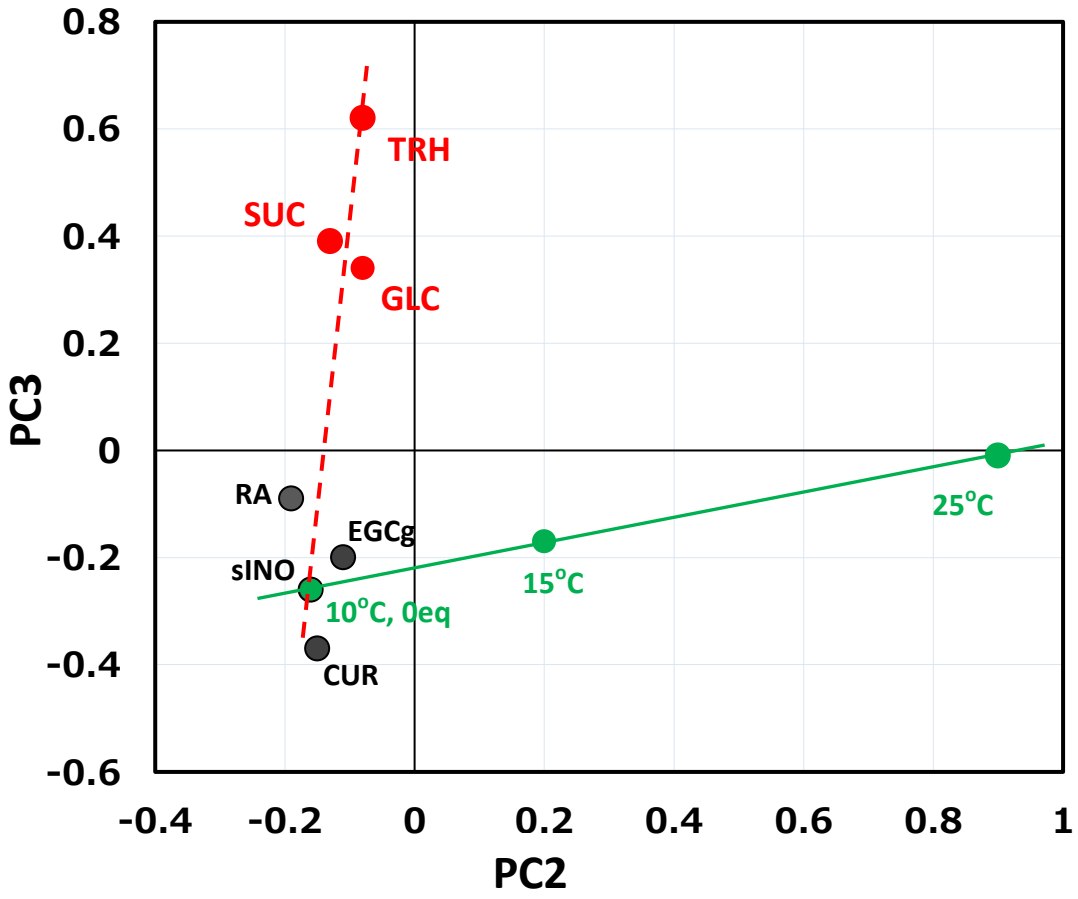
0.8
0.6
0.4
0.2
0
-0.2
-0.4
-0.6
PC3
-0.4
-0.2
0
0.2
0.4
0.6
0.8
1
PC2
TRH
SUC
GLC
RA
EGCg
sINO
10°C, 0eq
CUR
15°C
25°C

Figure 6